Towards symmetry driven and nature inspired UV filter design

Michael D. Horbury[†]*, Emily L. Holt[†§], Louis M. M. Mouterde[‡], Patrick Balaguer[#], Juan Cebrian~, Laurent Blasco~, Florent Allais[‡], and Vasilios G. Stavros[†]*

[†]Department of Chemistry, University of Warwick, Gibbet Hill, Coventry, CV4 7AL

[§]Molecular Analytical Science Centre for Doctoral Training, Senate House, University of Warwick, Coventry, CV4 7AL

[‡]URD Agro-Biotechnologies Industrielles (ABI), CEBB, AgroParisTech, 51110, Pomacle, France

[#]Institut de Recherche en Cancérologie de Montpellier, Campus Val d'Aurelle, 208 rue des Apothicaires, 34298 Montpellier Cedex 5, France

~Lubrizol Advanced Materials, C/Isaac Peral 17-Pol. Industrial Cami Ral, 08850 Gava, Spain

ABSTRACT: In plants, sinapate esters offer crucial protection from the deleterious effects of ultraviolet radiation exposure. These esters are a promising foundation for designing new sunscreen filters, particularly for the UVA (400 – 315 nm), where adequate photoprotection is currently lacking. Whilst sinapate esters are highly photostable due to a *cis*-*trans* (and *vice versa*) photoisomerization, the *cis*-isomer can display increased genotoxicity; an alarming concern for current cinnamate ester-based human sunscreens. To eliminate this potentiality, we have synthesised a sinapate ester with equivalent *cis*- and *trans*-isomers. We investigate its photostability through innovative ultrafast spectroscopy on a skin mimic, thus modelling the as-close-to true environment of sunscreen formulas. These studies are complemented by assessing endocrine disruption activity and antioxidant potential. We contest, from our results, that symmetrically functionalized sinapate esters may show exceptional promise as nature-inspired sunscreen filters in next generation sunscreen formulations.

Naturally occurring sinapate esters[1] have shown promise as starting points for a new generation of sunscreen filters, offering exemplary photoprotection. They exhibit high levels of photostability under ultraviolet (UV) exposure, due to an efficient *trans*-*cis* and *cis*-*trans* photoisomerization resulting in a photoequilibrium between these isomers, this process is shown in Fig. 1; starting from the *trans*-isomer of a sinapate ester as an example. More specifically, this photoisomerization after UV exposure, consists of three dynamical processes. After the initial absorption of UV radiation, the sinapate esters undergo a geometry relaxation. The geometry relaxation is then followed by the photoisomerization, which forms either the *cis*- or *trans*-isomer, and is mediated by a conical intersection between the excited state and ground electronic states.[2,3,4,5] During this relaxation, the excess electronic energy is converted into vibrational energy, leading to the isomers being formed vibrationally hot. This vibrational energy is eventually lost to the surrounding solvent bath.[6,7]

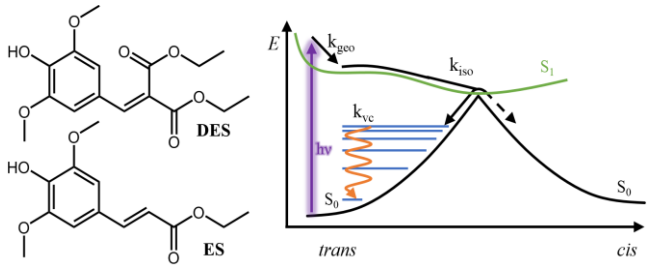


Fig. 1. The geometric structures of **DES** and **ES**, along with a schematic illustrating the dynamical processes involved in the photoisomerization of **ES**.

Not only do these sinapate esters display high UV photostability, they also demonstrate potent antioxidant capabilities.[8] However, they are not without their issues: Firstly, their absorption does not completely span the UVA region (400 – 315 nm), thus lacking optimum UVA photoprotection. Secondly, their UVA λ_{max} is close to the UVB (315 – 280 nm), of which there are already a plethora of effective UVB filters. Thirdly, the two isomers have differing absorption profiles, with the *cis*-isomer having the weaker absorption.[4,5,9] Fourthly, the genotoxicity of the *cis*-isomer has been shown to be significantly higher in a related cinnamate.[10] Lastly, concern has been raised over several other sunscreen filters being endocrine disruptors,[11,12,13,14] adding further considerations before any sinapate derivative can be included in a sunscreen formulation.

An intuitive solution to the issues introduced by the *cis*- and *trans*-isomer conundrum is to add identical ester moieties across the acrylic double bond, leading to indistinguishable *trans*- and *cis*-isomers. Concurrently, this serves to increase π-system conjugation and thus red-shift the λ_{max} (see Supplementary Fig. S1 for UV/visible spectra). To this end, we have synthesized diethyl 2-(4-hydroxy-3,5-dimethoxybenzylidene)malonate (diethyl sinapate) abbreviated **DES** hereon. **DES** is based on ethyl sinapate (**ES**) which has been previously studied by the Stavros group.[4] Structures of **DES** and **ES** are shown in Fig. 1.

However, while this spectral shift (to lower energy) in absorbance is a positive attribute towards **DES** being employed as a UVA filter, this alone does not indicate whether **DES** maintains the desired properties (*vide supra*) that may facilitate sinapate esters being promising sunscreen filters. Therefore, we have utilized a combination of femtosecond transient electronic (UV/visible) absorption spectroscopy (TEAS) and steady-state spectroscopy to investigate the photostability of **DES**. The combination of time-resolved and steady-state spectroscopies, enables one to link the ultrafast with the ultraslow dynamics, providing unprecedented insight into

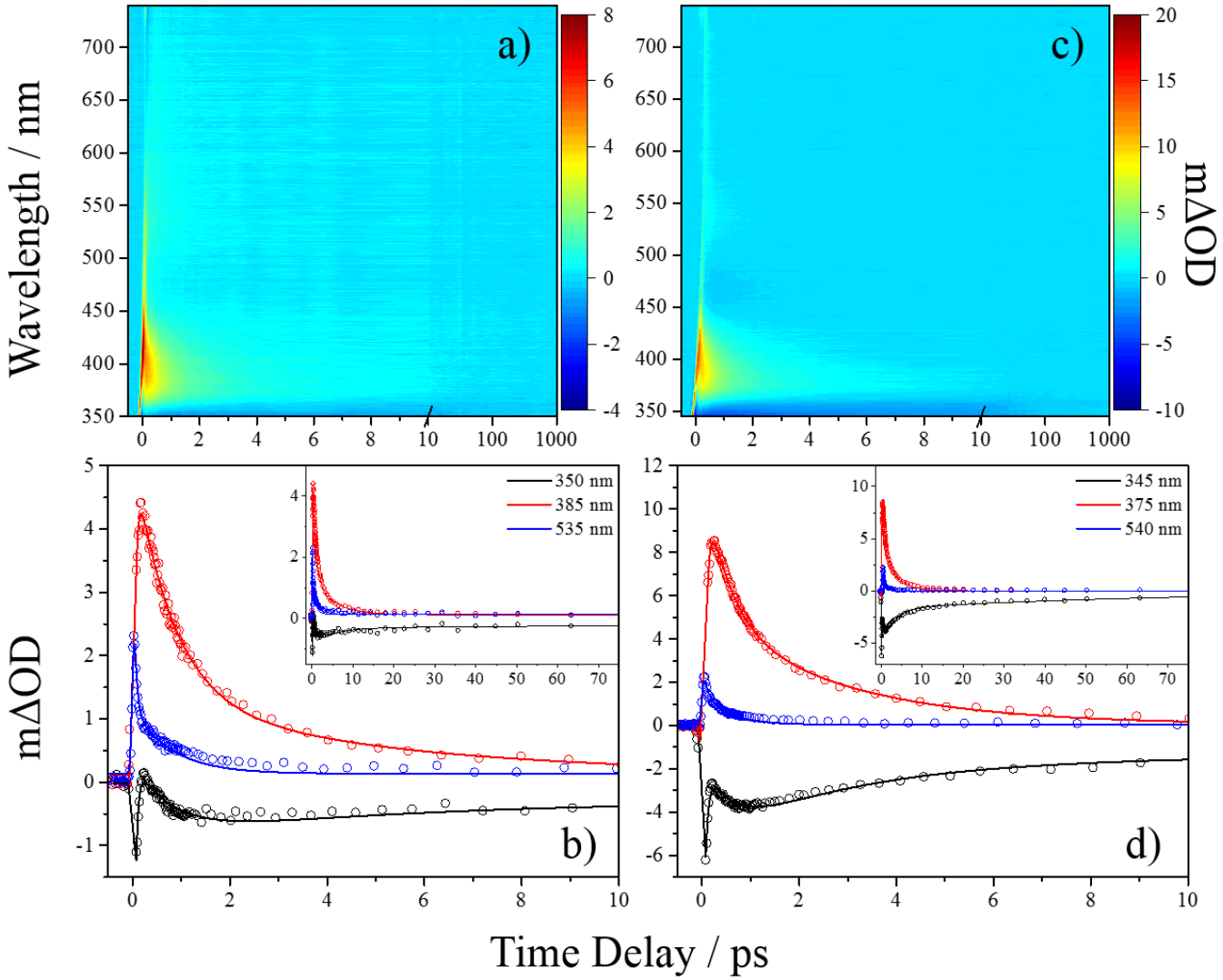


Fig. 2. TAS of **DES** in a) VC/AB and c) AB, both excited at 335 nm, shown as a false colourmap, with the intensity scale representing change in optical density (ΔOD). Note the x-scale is plotted linearly from -0.5 to 10 ps then as a log scale from 10 to 100 ps. Specific wavelength slices taken from the TAS of **DES** in b) VC/AB and d) AB, which have been globally fitted with a series of exponentials (k_n, $1 \leq n \leq 4$); the fits are shown by the solid line.

how photophysical processes involved at the very early stages of the photon-molecule interaction, influence the longer-term photostability.[2,3,4,5,7,15] TEAS measurements were taken of **DES** blended with a commercial sunscreen emollient, C12-15 alkyl-benzoate (AB) deposited on a synthetic skin mimic, VITRO-CORNEUM® (VC). The dynamical measurements taken using this innovative approach, makes the data accrued directly valid to real-world applications of sunscreen formulas.

While the present studies focus primarily on the spectroscopy of **DES**, we have not only developed two greener synthetic procedures to access **DES** but also carried out endocrine disruption measurements of **DES** for the alpha oestrogen receptor (ERα) and the xenobiotic receptor (PXR) as well as determining the antioxidant potential of **DES** using a 2,2-diphenyl-1-picrylhydrazyl (DPPH) assay. The combined results enable us to propose whether **DES** shows promise as a potentially new generation, nature-inspired sunscreening agent.

Results

Synthesis of DES. DES can be readily obtained through the Knoevenagel condensation of syringaldehyde and diethyl malonate. All the synthetic procedures that have been reported in the literature for such a condensation are not only quite hazardous, as they use toxic reagents/solvents such as piperidine and benzene, but they also require energy consuming-conventional heating. As we dedicate ourselves to the development of sustainable chemical pathways, our first goal was to design a greener synthesis of **DES**. By using microwave-heating instead of conventional heating, we were able to reduce energy consumption, eliminate benzene while reducing the reaction time from 7.5 hours to 30 minutes. Although this procedure brought significant improvements, it still required piperidine and column chromatography; moreover, one could also question the relevancy of microwaves at the industrial scale. A proline-mediated Knoevenagel-Doebner condensation in ethanol under conventional heating recently developed in our group was successfully implemented to the synthesis of DES at the multigram scale, thus allowing to fully replace piperidine. Finally, whatever the

synthetic procedure used (i.e., microwave-assisted or proline-mediated condensation), we also succeeded in replacing column chromatography purification by a simple precipitation.

Transient absorption spectroscopy. The transient absorption spectra (TAS) of **DES** in AB (10 mM) after being applied to the surface of VC (termed **DES** VC/AB hereon) and allowed to absorb into the substrate, are shown as a false colormap in Fig. 2a. Comparison TAS of **DES** in AB (1 mM) are also shown in Fig. 2c. We note the difference in initial **DES** concentration: this is due to the dilution of the sample as it absorbs into VC, meaning we are unable to accurately determine the concentration of **DES** in VC. That being said, due to the signal strength in the TAS (in comparison to the TAS for **DES** AB), we modestly estimate ~1.5 mM. Additional TAS were collected of **DES** in ethanol, cyclohexane and water (see Supplementary Fig. S2) to provide a range of solvent environments as comparisons. Saturated solutions (<1 mM) of **DES** in cyclohexane and water were used, while in ethanol a concentration of 1 mM was used. All samples were photoexcited at their UVA λ_{max}: VC/AB = 335 nm; AB = 335 nm; ethanol = 336 nm; cyclohexane = 325 nm; and water = 331 nm, (see Supplementary Fig. S1 for UV/visible spectra).

The excited state dynamics can be globally summarised by Fig. 1, with differences highlighted in the proceeding text where appropriate. After initial excitation, likely to a $^1\pi\pi^*$ state akin to what has been seen in **ES**,[4] the TAS of **DES** VC/AB and **DES** AB consists of a single excited state absorption which rapidly disappears within a pump-probe time-delay (Δt) of <100 fs (not apparent in Fig. 2, see Supplementary Fig. S3) as the excited population on the $^1\pi\pi^*$ state evolves from the initially prepared Franck-Condon region. This has been previously assigned to a combination of geometry relaxation (intramolecular vibrational redistribution) and solvent rearrangement,[16,17] and we conjecture a similar mechanism is in operation here. The geometry relaxation reveals three distinct spectral features that consist of: (i) a ground state bleach (~350 nm) corresponding to where the **DES** electronic ground state absorbs; (ii) a strong excited state absorption (~380 nm) and a second weaker excited state absorption (~540 nm); and (iii) a stimulated emission (~470 nm,). We note for **DES** VC**/**AB that this feature is very weak (<0.2 mΔOD) and have elected to not include this feature in our global fitting (see below). (i)-(iii) are in accordance with what has been observed from $^1\pi\pi^*$ state-driven dynamics for **ES**.[4]

As the TAS evolve in time, the excited state absorption and stimulated emission have decayed by Δt = ~4 ps. Thereafter a small absorption at ~380 nm and the ground state bleach features remain. The decay of the excited state absorption and stimulated emission is attributed to repopulation of the electronic ground state from the $^1\pi\pi^*$ state, likely mediated by a photoisomerization pathway.[4] This photoisomerization pathway leads to the electronic ground state being vibrationally populated. Therefore, we attribute the small absorption peak at ~380 nm to the absorption from this vibrationally hot electronic ground state. As this state 'cools' to the solvent bath, the peak at ~380 nm decays completely. However, the corresponding ground state bleach remains. Crucially, this *has not* been previously seen in **ES** or any related sinapate or cinnamate in the condensed phase.[2,4,5,7,15,18] The ground state bleach eventually recovers, suggesting that the population of a "dark" state acts (in competition with other pathways) as an intermediary electronic excited state en route to electronic ground state repopulation. We discuss this in more detail below.

Table 1. Rate-constants (k_n) resulting from the fitting of selected wavelength transients of the TAS of **DES** in VC/AB, and AB. The errors are quoted to 2σ.

	k_{geo} / s^{-1} ($x10^{13}$)	k_{iso} / s^{-1} ($x10^{12}$)	k_{vc} / s^{-1} ($x10^{11}$)	k_{dark} / s^{-1} ($x10^{10}$)
VC/AB	2 ± 1.6	1.2 ± 0.1	2.0 ± 0.2	0.4 ± 0.2
AB	1.7 ± 1.1	1.9 ± 0.2	3.6 ± 0.1	1.4 ± 0.2

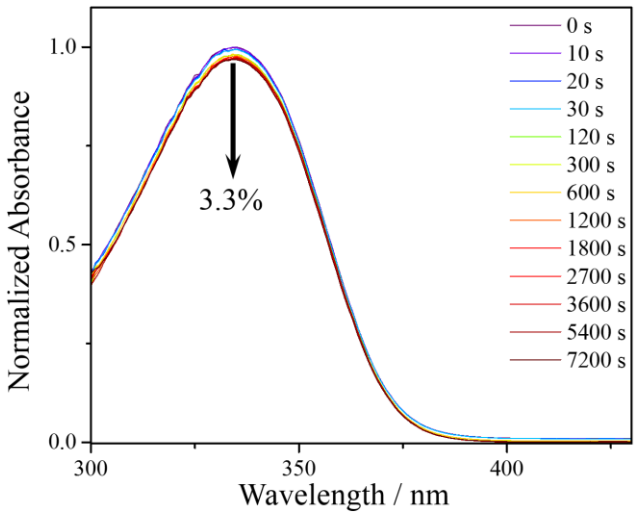


Fig. 3. UV/visible spectra of **DES** in AB, at varying durations of irradiation at 335 nm and replicating solar intensity.

From the TAS presented (see Fig 2) three distinct and separate features were chosen to model the kinetics (photodynamical processes) of **DES**; in VC/AB and AB. The three features chosen were the ground state bleach (~350 nm), the large excited state absorption (~380 nm) and the weak excited state absorption (~540 nm). These spectral features (S) were simultaneously (globally) fit using the following equation:

$$S(\Delta t) = \sum_{n=1}^{4} g(\Delta t) * \left(C_n exp(-\Delta t * k_n)\right)$$

Here, $g(\Delta t)$ is our Gaussian instrument response function (~80 fs) and k_n is the rate constant for the geometry relaxation (k_{geo}; n = 1), photoisomerization (k_{iso}; n = 2), vibrational cooling (k_{vc}; n = 3) and the decay of the "dark" state (k_{dark}; n = 4). C_n are the amplitudes of each exponential component and only these were allowed to vary during the global fit. Furthermore, only the ground state bleach is affected by all four dynamical process. Therefore, C_4 is fixed to zero for the strong and weak excited state absorption as these are not affected by the "dark" state. In addition, C_3 is also set to zero for the weak excited state absorption. The value for each rate-constant attained is shown in Table 1.

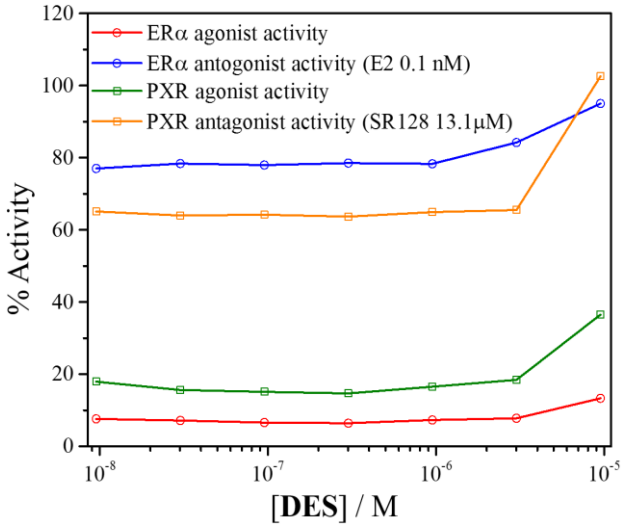


Fig. 4. Endocrine disruption activity of **DES** for ERα (circle) as either an agonist (red) or antagonist (blue) and for PXR (square) as either an agonist (green) or antagonist (orange).

Steady-state spectroscopy. To complement the time-resolved measurements, steady-state irradiation measurements were carried out, to determine the long-term photostability of **DES**. UV/visible spectra were taken at various time-intervals during the irradiation of the sample at its UVA λ_{max} at solar intensity (0.2 mWcm^{-2}). The resulting UV/visible spectra of **DES** in AB are shown in Fig. 3. It is clear from these spectra that over a period of two hours, **DES** only experiences a minor reduction in its absorbance, 3.3%, while for the UVA λ_{max} of ethanol, water and cyclohexane a drop of 3.1%, 2.4% and 1.6%, respectively, was observed (see Supplementary Fig. S4 for additional spectra). Hampered by scattering issues within the spectrometer, we were unable to perform these measurements for **DES** VC/AB. For comparison, *trans*-**ES** in cyclohexane experiences a 16% loss in absorbance over a period of 45 minutes, a consequence of establishing a photoequilibrium between the two (*trans* and *cis*) structural isomers.[4]

Endocrine disruption potential of DES. Endocrine disruption activity of **DES** was assayed on two types of receptors. The first receptor selected was the ERα receptor, which is a member of the nuclear hormone receptors family, whose activity is regulated by the steroid and oestrogen sex hormone 17β-estradiol (E2). The second receptor is the PXR receptor, a member of the steroid and xenobiotic sensing nuclear receptors family, with a known agonist being SR 12813. Endocrine disruption assays, shown in Fig. 4, demonstrate that DES is neither an agonist nor antagonist ligand for either ERα or PXR.

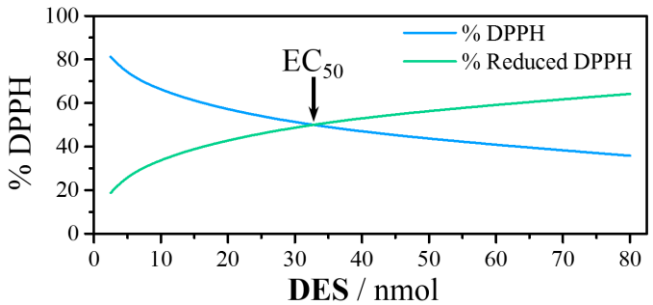


Fig. 5. Antiradical activity determination *via* DPPH assay, the EC_{50} is provided by the crossing point of % DPPH (blue) and % reduced DPPH) (green), which occurs at 32.7 nmol.

Antioxidant potential of DES. While the photostability of sinapates is a major interest for use as sunscreen filters, their potent antioxidant capabilities are an added benefit. Therefore, to determine if **DES** also exhibits antioxidant potential, a DPPH assay was carried out. This method determines the H-donor capacity of the antioxidant to quench the stable DPPH free radical, as previously reported.[8] In this study, the EC_{50} value (lower is better) corresponds to the amount of antioxidant, needed to reduce half of the initial population of DPPH radicals. The lower the EC_{50} value, the higher the antioxidant potential. **DES**'s EC_{50} value was determined as being 32.7 nmol, as highlighted in Fig. 5. For ease of comparison with other studies we have converted this value to a ratio, quoted as [antioxidant]/[DPPH]; this gives a value of 0.86 for **DES**, we will discuss this value with regards to widely used commercially available antioxidants.

DPPH studies:

	Irganox 1010	Trolox	BHT	BHA	ES	DES
EC_{50} (nmol)	6.89	4.02	7.11	3.67	13.7	32.7
[antioxidant]/[DPPH]	0.18	0.11	0.19	0.10	0.36	0.86

Discussion

The spectroscopic measurements, both time-resolved and steady-state, have demonstrated that the addition of the second ester moiety has not impeded the high UV photostability that the sinapate backbone possesses.[4] This is highlighted by the minimal drop (≤3.3%) in the absorbance of **DES** after 2 hours of UV irradiation, at solar intensities.

Interestingly however, an additional ground state recovery pathway is observed in the TEAS measurements of **DES**. This process appears as an extended recovery in the ground state bleach in the TAS (*vide supra*, Fig. 2b and d), with no other spectral features associated with it. Their absence is either due to their spectral features being outside of the TEAS spectral probe window, or weak absorption from this state to higher lying electronic states within the probe window. We believe that this is most likely an $^1n\pi^*$ state, another electronic excited state that has previously been implicated to play a role in the photodynamics of cinnamates.[19,20,21] Whether the population of this excited state happens concomitantly with the photoisomerization back to the electronic ground state or is due to a bifurcation of the excited state population after initial excitation is unknown.

Furthermore, there is an apparent viscosity dependence on the decay of this "dark" state, which is best highlighted by the difference in k_{dark} between **DES** in AB (η = 38) and ethanol (η = 1.19)[22] where k_{dark} is 4 times quicker in ethanol. Interestingly k_{iso} is not affected by solvent viscosity (see Supplementary Information for k_{dark} and k_{iso} for **DES** in ethanol). In a previous

study on sinapate esters, the rate of photoisomerization has been shown to be impacted by the viscosity,[3] attributed to the large amplitude nuclear motion that occurs during the photoisomerization. The absence of a viscosity effect on k_{iso} does not rule out photoisomerization, however, as related cinnamates, that undergo photoisomerization, also show no viscosity dependence due to the in plane motion during the isomerization.[16,17] Yet, the dependence for k_{dark} does suggest that the relaxation pathway of this "dark" state involves significant nuclear motion, whether this is also a photoisomerization or some other nuclear motion is unclear. We also note that **DES** in VC/AB also impacts k_{dark}, to a greater extent than in AB; this serves to highlight the importance of using a more realistic model for these measurements. Ultimately, while this additional decay pathway is present, it does not appear to impact the long-term photostability of **DES**. Characterisation of this state and how it is populated will inevitably benefit from high level theoretical and (supplementary) experimental work, the latter utilizing different probe techniques, to elucidate how the excited state population evolves in **DES**. This, however, is beyond the scope of the current work.

Another consideration in whether **DES** shows promise as a next generation sunscreening agent is if it is an endocrine disruptor which has previously caused controversies for current UV filters.[11,12,14] Due to these controversies and the general concern over endocrine disrupting chemicals,[23] it is becoming a significant factor in the design of new sunscreening agents. Fortunately, in the case of **DES** the endocrine disruption measurements showed no adverse effects to the ERα or PXR receptors.

Whilst the intrinsic UV photostability of the sinapates is a draw for them as sunscreen filters, their potent antioxidant potential is an additional benefit. Whilst the DPPH assays demonstrate that **DES** can act as an antioxidant, its activity (0.86) is lower than **ES** (0.36),[8] Irganox1010 (0.18), Trolox (0.11), BHT (0.19), BHA (0.10) and α-tocopherol (0.21),[24] the latter being an antioxidant used in commercial sunscreen formulations. α-tocopherol is only included in sunscreening formulas in small quantities compared to sunscreen filters. Therefore, while the antioxidant potential of **DES** is lower, its concentration will be significantly greater. Coupled to its low endocrine disruption activity, this provides undeniably evidence that **DES** shows promise as a candidate ingredient for the next generation sunscreen filter with dual (*vide supra*) functionality.

Amidst growing concerns of increasing exposure of society to solar radiation, the results presented herein demonstrate the promising new potential of sinapate ester sunscreens for commercial use in sunscreen formulations. The symmetric functionalisation across the acrylic double bond ensures that the *cis*- and *trans*-isomers are equivalent, negating concerns over genotoxicity of isomeric photoproducts. Concurrently, the absorption has been spectrally shifted into the UVA region, where there is a growing need for sunscreen filters. Moreover, the photodynamics measured for **DES** in an emollient used in commercial sunscreen formulas are consistent when also deposited on a synthetic skin mimic. This provides confidence of the photoprotection potential of **DES** in a real-world setting. Our work provides a blueprint for further modifications to the ester group functionality to potentially add additional beneficial properties (*e.g.* enhanced antioxidant potential), especially given the modest impact on the photochemistry when changing the ester group functionality.[2,3,4,7] This ability for customization has broad implications for not only human photoprotection, but for materials under constant UV exposure such as plastics and resins. Finally, **DES** displays no endocrine disruption activity, which is a significant requirement in next generation sunscreens filters given ever-growing concerns over current sunscreen filters on both human health and aquatic life.[11,12,13,14]

Methods

Synthesis.

DES was synthesized in one step using either a micro-wave-assisted or a proline-mediated Knoevenagel condensation between lignin-derived syringaldehyde and diethyl malonate (Scheme 1).[25]

Procedure 1:

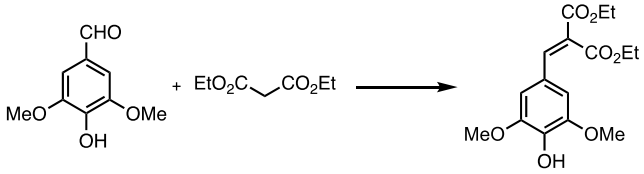
Syringaldehyde (4 mmol, 728 mg) and diethylmalonate (13 mmol, 2 mL) were mixed together. Piperidine (2 mmol, 200 µL) was then added to the reaction mixture, the tube sealed and placed into a Monowave 400 microwave system. Constant power (50 W) was applied until reaching a temperature of 100 °C which was then maintained for 30 additional minutes. The reaction mixture was directly purified by flash chromatography (Cyclohexane/Ethyl acetate 8/2). Fraction containing the wanted product was evaporated under vacuum to afford pure **DES** (1.1 g, 85%).

Procedure 2:

Syringaldehyde (4 mmol, 728 mg) and diethylmalonate (13 mmol, 2 mL) were mixed together. Piperidine (2 mmol, 200 µL) was then added to the reaction mixture, the tube sealed and placed into a Monowave 400. Constant power (50 W) was applied until reaching a temperature of 100 °C which was then maintained for 30 additional minutes. The reaction mixture was cooled down to room temperature and added dropwise to a 1N HCl aqueous solution (50 mL) at 0 °C. The resulting precipitate was filtered and washed with cold water to afford pure **DES** (1.05 g, 80%).

Procedure 3:

Syringaldehyde (4 mmol, 728 mg) and diethylmalonate (13 mmol, 2 mL) were mixed together. Proline (2 mmol, 235 mg) was then added and the reaction mixture was refluxed overnight. The reaction mixture was cooled down to room temperature and added dropwise to a 1N HCl aqueous solution (50 mL) at 0 °C. The resulting precipitate was filtered and washed with cold water to afford pure **DES** (1.04 g, 80%).



Scheme 1. DES synthesis through Knoevenagel condensation.

Spectroscopy.

The TEAS setup used to observe the photochemistry of **DES** has been described in detail previously,[26,27] however, information specific to the present experiments is provided herein. Samples of **DES** were made to a concentration of 1 mM in C12–15 alkyl benzoate (Lubrizol), ethanol (absolute, VWR), Water (deionized) and cyclohexane (99.99%, VWR). For **DES** on VITRO-CORNEUM® (IMS Inc.) a **DES** sample at a concentration of 10 mM in C12–15 alkyl benzoate was applied to VITRO-CORNEUM®. The fs pump pulses were generated by an optical parametric amplifier (TOPAS-C, Spectra-Physics) with a fluence of 200 – 800 μJ·cm^{-2}. The probe pulse was a broadband white light supercontinuum generated in a vertically translated CaF_2 window, providing a probe spectral window of 345 – 735 nm. The pump-probe time delay (Δt) was varied by adjusting the optical delay of the probe pulse, the maximum obtainable Δt was 2 nanoseconds (ns). Changes in the optical density (ΔOD) of the samples were calculated from transmitted probe intensities, collected using a spectrometer (Avantes, AvaSpec-ULS1650F). The sample delivery system was a flow-through cell (Demountable Liquid Cell by Harrick Scientific Products Inc.) consisting of two CaF_2 windows; the windows where spaced 100 μm apart. The sample was circulated using a diaphragm pump (SIMDOS, KNF) and replenished from a 25 mL reservoir to provide each pulse-pair with fresh sample. For VC/AB the sample thickness was measured to be 120 μm and was mounted on the front of a CaF_2 window.

Steady-state UV/vis absorption spectra of **DES** in AB, ethanol, water and cyclohexane, were using a UV/vis spectrometer (Cary 60, Agilent Technologies). The samples were irradiated with an arc lamp (Fluorolog 3, Horiba) for 2 hours, with the UV/vis spectra taken at various time points, at the corresponding TEAS excitation wavelength, using an 8 nm bandwidth of the irradiation source. The fluence was set to 100 – 200 μJ·cm^{-2} to mimic solar incidence conditions.

Endocrine disruption measurements.

Cell culture material was from Life Technologies (Cergy-Pontoise, France) except the 96-well Cell star plates, which were from Greiner Labortechnic (Poitiers, France). Luciferin (sodium salt) and geneticin were purchased from Promega (Charbonnières, France). R1881 was from NEN Life Science Products (Paris, France). Estradiol, SR12813, hygromycin and puromycin were purchased from Sigma Aldrich (Saint-Quentin Fallavier, France). Stocks solutions were made in dimethyl sulfoxide (DMSO) at 10 mM and dilutions from this stock solution were prepared in a culture medium.

HELN and HELN hERα cells were already described.[28] Briefly, Hela cells were stably transfected with the ERE-βGlobin-Luciferase-SVNeomycin plasmid, with or without the pSG5-hERα-puromycin plasmid leading to the HELN and HELN hERα-cell lines. HG5LN and HG5LN PXR cells were already described.[29] The Hela cells were stably transfected with the $GAL4RE_5$-βGlobin-Luciferase-SVNeomycin plasmid, with or without the pSG5-GAL4(DBD)-hPXR(LBD)-puromycin plasmid leading to the HG5LN and HG5LN-hPXR cell lines.

Cells were cultured at 37 °C under humidified 5% CO_2 atmosphere. HG5LN, HG5LN PXR and HELN cells were cultured in red phenol (DMEM)-F12 medium (Thermofisher, Villebon sur Yvette, France) supplemented with 1% penicillin/streptomycin and 5% fetal calf serum (FCS). HELN hERα cells were cultured in DMEM-F12 without red phenol supplemented with penicillin/streptomycin (1%) and dextran-coated charcoal-treated fetal calf serum (DCC-FCS) (5%) (Test medium)

Cells were seeded in 96-well white opaque flat bottom plates at 25,000 cells per well in 150 μL of test medium. **DES** (four replicates per plate) was added 24h later using automated workstation (Biomek 3000, Beckman Coulter, Villepinte, Paris) and cells were incubated at 37 °C for 16h. Then, the medium was removed and 50 μL of test medium containing luciferin at 0.3 mM was added per well. After 5 min, the production of light was measured in living cells using microplate luminometer (MicroBeta, PerkinElmer SAS, Courtaboeuf, France).

Agonistic activities of HELN hERα and HG5LN hPXR cells were tested in the presence of increasing concentrations (10nM-10μM) of **DES**. Results were expressed as a percentage of maximal luciferase activity. Maximal luciferase activity (100%) was obtained in the presence of 10 nM E2 for ERα, and 3 μM SR12813 for PXR. Antagonistic assays were performed using a concentration of agonist yielding approximately 60-85% of maximal luciferase activity. The antagonistic activity of **DES** tested at (10 nM – 10 μM) was determined by co-incubation with the agonist E2 at 0.1nM for ERα, and the agonist SR12813 at 100 nM for PXR.

DES was also tested for non-specific modulation of luciferase expression on the HELN and HG5LN cell line, which are devoid of hERα and hPXR. **DES** showed non-specific induction of luciferase expression at 10 μM.

Antioxidant measurements.

190 μL of homogeneous DPPH solution (200 μM) in ethanol was added to a well containing 10 μL of the potential anti-radical molecule solution in ethanol at different concentrations (from 400 μM to 12.5 μM). The reaction was followed by a microplate Multiskan FC, performing 1 scan every 5 min for 7.5 h at 515 nm. The use of different amounts of **DES** give the EC_{50} value, which is describe as the efficient concentration needed to reduce the initial population of DPPH by half.

This procedure has been applied to commercially available antioxidants to provide not only positive controls but also benchmark values: Irganox1010 antioxidant used in polymers, Trolox antioxidant used in the pharmaceutical industry, BHT and BHA antioxidants used in the cosmetic and food/feed industries.

Supporting Information

UV/visible absorption spectra, additional transient absorption spectroscopy measurements, Synthesis of **DES**.

AUTHOR INFORMATION

Author Contribution

M.D.H and E.L.H acquired and analysed the time-resolved and steady-state spectroscopic data and prepared the manuscript. L.M.M.M, P.B and F.A conceived and performed the synthesis, conducted DPPH assay and endocrine disruption measurements as well as contributing to the preparation of the manuscript. J.C and L.B provided invaluable direction for modelling a closer-to-realistic sunscreen environment (synthetic skin mimic) as well as critiquing the manuscript. V.G.S conceived the experiments and provided guidance in data analysis and interpretation, and the writing of the manuscript.

Corresponding Authors

Emails: v.stavros@warwick.ac.uk and m.horbury@warwick.ac.uk

Notes

The authors declare no competing financial interests.

ACKNOWLEDGMENTS

The authors would like to thank the Warwick Centre for Ultrafast Spectroscopy (WCUS) for the use of the Cary 60 and Fluorolog 3. M. D. H. thanks the Leverhulme Trust for postdoctoral funding. E. L. H. thanks the EPSRC for a PhD studentship through the EPSRC Centre for Doctoral Training in Molecular Analytical Science, grant number EP/L015307/1. L. M. M. M. and F. A. thank the ANR for the SINAPUV grant (ANR-17-CE07-0046), and the Grand Reims, the Conseil Départemental de la Marne and the Region Grand Est for financial support. Finally, V. G. S. thanks the EPSRC for an equipment grant (EP/J007153), the Leverhulme Trust for a research grant (RPG-2016-055) and the Royal Society and Leverhulme Trust for a Royal Society Leverhulme Trust Senior Research Fellowship.

REFERENCES

1. Dixon RA, Achnine L, Kota P, Liu CJ, Reddy M, Wang L. The phenylpropanoid pathway and plant defence—a genomics perspective. *Molecular plant pathology* 2002, **3**(5)**:** 371-390.
2. Baker LA, Horbury MD, Greenough SE, Allais F, Walsh PS, Habershon S*, et al.* Ultrafast Photoprotecting Sunscreens in Natural Plants. *J Phys Chem Lett* 2016, **7**(7)**:** 56-61.
3. Horbury M, Quan W-D, Flourat A, Allais F, Stavros V. Elucidating nuclear motions in a plant sunscreen during photoisomerization through solvent viscosity effects. *Phys Chem Chem Phys* 2017, **19**(31)**:** 21127-21131.
4. Horbury M, Flourat AL, Greenough SE, Allais F, Stavros V. Investigating isomer specific photoprotection in a model plant sunscreen. *Chem Commun* 2018, **54:** 936-939.
5. Luo J, Liu Y, Yang S, Flourat AL, Allais F, Han K. Ultrafast Barrierless Photoisomerization and Strong Ultraviolet Absorption of Photoproducts in Plant Sunscreens. *J Phys Chem Lett* 2017, **8:** 1025-1030.
6. Horbury MD, Baker LA, Rodrigues ND, Quan W-D, Stavros VG. Photoisomerization of ethyl ferulate: A solution phase transient absorption study. *Chem Phys Lett* 2017, **673:** 62-67.
7. Baker LA, Staniforth M, Flourat A, Allais F, Stavros V. Gas-Solution Phase Transient Absorption Study of the Plant Sunscreen Derivative Methyl Sinapate. *ChemPhotoChem* 2018.
8. Reano AF, Chérubin J, Peru AlM, Wang Q, Clement T, Domenek S*, et al.* Structure–activity relationships and structural design optimization of a series of p-hydroxycinnamic acids-based bis-and trisphenols as novel sustainable antiradical/antioxidant additives. *ACS Sustainable Chemistry Engineering* 2015, **3**(12)**:** 3486-3496.
9. Challice JS, Williams AH. Paper Chromatographic Separation and Behavior of the cis-and trans-Isomers of Cinnamic Acid Derivatives. *J Chromatogr A* 1966, **21:** 357-362.
10. Sharma A, Bányiová K, Babica P, El Yamani N, Collins AR, Čupr P. Different DNA damage response of cis and trans isomers of commonly used UV filter after the exposure on adult human liver stem cells and human lymphoblastoid cells. *Science of the Total Environment* 2017, **593:** 18-26.
11. Burnett ME, Wang SQ. Current Sunscreen Controversies: A Critical Review. *Photodermatol Photoimmunol Photomed* 2011, **27**(2)**:** 58-67.
12. Loden M, Beitner H, Gonzalez H, Edström DW, Åkerström U, Austad J*, et al.* Sunscreen Use: Controversies, Challenges and Regulatory Aspects. *Br J Dermatol* 2011, **165**(2)**:** 255-262.
13. Skotarczak K, Osmola-Mańkowska A, Lodyga M, Polańska A, Mazur M, Adamski Z. Photoprotection: Facts and Controversies. *Eur Rev Med Pharmacol Sci* 2015, **19**(1)**:** 98-112.
14. Krause M, Klit A, Blomberg Jensen M, Søeborg T, Frederiksen H, Schlumpf M*, et al.* Sunscreens: are they beneficial for health? An overview of endocrine disrupting properties of UV-filters. *International journal of andrology* 2012, **35**(3)**:** 424-436.
15. Vengris M, Larsen DS, van der Horst MA, Larsen OFA, Hellingwerf KJ, van Grondelle R. Ultrafast Dynamics of Isolated Model Photoactive Yellow Protein Chromophores: "Chemical Perturbation Theory" in the Laboratory. *J Phys Chem B* 2005, **109**(9)**:** 4197-4208.
16. Espagne A, Paik DH, Changenet-Barret P, Martin MM, Zewail AH. Ultrafast Photoisomerization of Photoactive Yellow Protein Chromophore Analogues in Solution: Influence of the Protonation State. *ChemPhysChem* 2006, **7**(8)**:** 1717-1726.
17. Kuramochi H, Takeuchi S, Tahara T. Ultrafast Structural Evolution of Photoactive Yellow Protein Chromophore Revealed by Ultraviolet Resonance Femtosecond Stimulated Raman Spectroscopy. *J Phys Chem Lett* 2012, **3**(15)**:** 2025-2029.
18. Peperstraete Y, Staniforth M, Baker LA, Rodrigues ND, Cole-Filipiak NC, Quan W-D*, et al.* Bottom-up excited state dynamics of two cinnamate-based

sunscreen filter molecules. *Phys Chem Chem Phys* 2016, **18**(40)**:** 28140-28149.
19. Karsili TNV, Marchetti B, Ashfold MNR, Domcke W. *Ab Initio* Study of Potential Ultrafast Internal Conversion Routes in Oxybenzone, Caffeic Acid and Ferulic Acid: Implications for sunscreens. *J Phys Chem A* 2014, **118**(51)**:** 11999-12010.
20. Rodrigues NDN, Staniforth M, Young JD, Peperstraete Y, Cole-Filipiak NC, Gord J*, et al.* Towards elucidating the photochemistry of the sunscreen filter ethyl ferulate using time-resolved gas-phase spectroscopy. *Farad Discuss* 2016.
21. Molina V, Merchán M. On the absorbance changes in the photocycle of the photoactive yellow protein: a quantum-chemical analysis. *Proc Natl Acad Sci* 2001, **98**(8)**:** 4299-4304.
22. Khattab IS, Bandarkar F, Fakhree MAA, Jouyban A. Density, viscosity, and surface tension of water+ ethanol mixtures from 293 to 323K. *Korean Journal of Chemical Engineering* 2012, **29**(6)**:** 812-817.
23. Colborn T, Vom Saal FS, Soto AM. Developmental effects of endocrine-disrupting chemicals in wildlife and humans. *Environmental health perspectives* 1993, **101**(5)**:** 378-384.
24. Mishra K, Ojha H, Chaudhury NK. Estimation of antiradical properties of antioxidants using DPPH assay: A critical review and results. *Food chemistry* 2012, **130**(4)**:** 1036-1043.
25. Mouterde LM, Allais F. Microwave-Assisted Knoevenagel-Doebner Reaction: An Efficient Method for Naturally Occurring Phenolic Acids Synthesis. *Frontiers in chemistry* 2018, **6**.
26. Greenough SE, Horbury MD, Thompson JOF, Roberts GM, Karsili TNV, Marchetti B*, et al.* Solvent Induced Conformer Specific Photochemistry of Guaiacol. *Phys Chem Chem Phys* 2014, **16**(30)**:** 16187-16195.
27. Greenough SE, Roberts GM, Smith NA, Horbury MD, McKinlay RG, Żurek JM*, et al.* Ultrafast Photo-Induced Ligand Solvolysis of cis-[Ru (bipyridine)$_2$(nicotinamide)$_2$]$^{2+}$: Experimental and Theoretical Insight into its Photoactivation Mechanism. *Phys Chem Chem Phys* 2014, **16**(36)**:** 19141-19155.
28. Delfosse V, Grimaldi M, Pons J-L, Boulahtouf A, Le Maire A, Cavailles V*, et al.* Structural and mechanistic insights into bisphenols action provide guidelines for risk assessment and discovery of bisphenol A substitutes. *Proc Natl Acad Sci USA* 2012, **109**(37)**:** 14930-14935.
29. Delfosse V, Dendele B, Huet T, Grimaldi M, Boulahtouf A, Gerbal-Chaloin S*, et al.* Synergistic activation of human pregnane X receptor by binary cocktails of pharmaceutical and environmental compounds. *Nature communications* 2015, **6:** 8089.

Table of Content

